Rab8a Deficiency in Skeletal Muscle Causes Hyperlipidemia and Hepatosteatosis by Impairing Muscle Lipid Uptake and Storage

Qiaoli Chen,[1] Ping Rong,[1] Dijin Xu,[2] Sangsang Zhu,[1] Liang Chen,[1] Bingxian Xie,[1] Qian Du,[1] Chao Quan,[1] Yang Sheng,[1] Tong-Jin Zhao,[3] Peng Li,[2] Hong Yu Wang,[1] and Shuai Chen[1]

Diabetes 2017;66:2387–2399 | https://doi.org/10.2337/db17-0077

Skeletal muscle absorbs long-chain fatty acids (LCFAs) that are either oxidized in mitochondria or temporarily stored as triglycerides in lipid droplets (LDs). So far, it is still not fully understood how lipid uptake and storage are regulated in muscle and whether these are important for whole-body lipid homeostasis. Here we show that the small GTPase Rab8a regulates lipid uptake and storage in skeletal muscle. Muscle-specific Rab8a deletion caused hyperlipidemia and exacerbated hepatosteatosis induced by a high-fat diet. Mechanistically, Rab8a deficiency decreased LCFA entry into skeletal muscle and inhibited LD fusion in muscle cells. Consequently, blood lipid levels were elevated and stimulated hepatic mammalian target of rapamycin, which enhanced hepatosteatosis by upregulating hepatic lipogenesis and cholesterol biosynthesis. Our results demonstrate the significance of lipid uptake and storage in muscle in regulating whole-body lipid homeostasis, and they shed light on the roles of skeletal muscle in the pathogenesis of hyperlipidemia and hepatosteatosis.

Metabolic diseases including obesity, type 2 diabetes, and nonalcoholic fatty liver disease (NAFLD) have recently become prevalent worldwide, which urges a better understanding of their pathogenesis in order to improve their prevention and treatment. Skeletal muscle, as the largest organ in the human body, has a critical role in regulating whole-body metabolic homeostasis (1), though its roles in the pathogenesis of metabolic diseases are still not fully understood.

After a meal, nutrients including glucose and lipids surge into the blood. Up to 70% of postprandial glucose is absorbed by skeletal muscle and stored as glycogen; this critical process maintains blood glucose levels (1). Mainly GLUT4 mediates the entry of glucose into skeletal muscle; GLUT4 can translocate from its intracellular storage sites onto the plasma membrane in response to insulin (2). Insulin also stimulates translocation of the fatty acid translocase CD36 onto the plasma membrane to mediate uptake of long-chain fatty acids (LCFAs) in skeletal muscle (3,4). Once absorbed, LCFAs can be channeled into the mitochondria for oxidation (5) or esterified to form triglycerides for storage in lipid droplets (LDs) (6). LDs are cytoplasmic organelles that have a phospholipid monolayer surrounding a neutral lipid core comprising triglycerides and/or cholesterol esters (7). Although skeletal muscle is not classically considered to be an important organ in lipid storage, its lipid stores can make up ~8% of total body lipids (8). Under conditions of a high-fat diet (HFD), skeletal muscle can accumulate more neutral lipids with enlarged LDs (9,10).

Rab8a is a small GTPase that plays crucial roles in membrane trafficking and may be involved in regulating both lipid and glucose metabolism. Rab8a deficiency inhibits nutrient absorption in the small intestine and causes premature death in mice as a result of apical proteins such as peptidases and transporters mislocalized to the lysosome for degradation in intestinal epithelial cells (11). Rab8a has been implicated in the regulation of insulin-stimulated GLUT4 translocation

[1]MOE Key Laboratory of Model Animal for Disease Study and State Key Laboratory of Pharmaceutical Biotechnology, Model Animal Research Center, Nanjing University, Pukou District, Nanjing, China
[2]Tsinghua-Peking Center for Life Sciences, School of Life Sciences, Tsinghua University, Beijing, China
[3]State Key Laboratory of Cellular Stress Biology, School of Life Sciences, Xiamen University, Xiamen, Fujian, China

Corresponding author: Hong Yu Wang, wanghy@nicemice.cn, or Shuai Chen, schen6@163.com.

Received 16 January 2017 and accepted 21 June 2017.

This article contains Supplementary Data online at http://diabetes.diabetesjournals.org/lookup/suppl/doi:10.2337/db17-0077/-/DC1.

H.Y.W. and S.C. are co–senior authors.

Q.C. and P.R. are co–first authors.

in L6 muscle cells (12,13) and CD36 translocation in HL-1 cardiomyocytes (14). Downregulation of Rab8a via small interfering RNA (siRNA) inhibits insulin-stimulated translocation of GLUT4 or CD36 in these culture cells (12–14). LDs can grow in size through either two smaller LDs fusing into one larger LD (15) or neutral lipids being added to preexisting droplets (16). Rab8a also has been shown to regulate LD fusion in 3T3-L1 adipocytes (17). Given the importance of LDs and insulin-stimulated translocation of GLUT4 and CD36 in skeletal muscle, we hypothesize that Rab8a may have a critical metabolic role in skeletal muscle, which may influence whole-body metabolic homeostasis. In this study, we took a genetic approach to investigate the impacts of Rab8a deficiency in skeletal muscle on metabolic homeostasis in this tissue and at the whole-body level.

RESEARCH DESIGN AND METHODS

Materials

Recombinant human insulin was purchased from Novo Nordisk (Bagsvaerd, Denmark). Rapamycin (S1039) and fenofibrate (S1794) were from Selleck Chemicals. Borondipyrromethene (BODIPY) 493/503 (D-3922) and BODIPY 558/568 C12 (D-3835) were from Thermo Fisher Scientific. 2-Deoxy-D-[1,2-^{3}H(N)]glucose, D-[1-^{14}C]-mannitol, and [^{14}C(U)]-palmitic acid were from PerkinElmer. All other chemicals were from Sigma-Aldrich or Sangon Biotech Co. Ltd (Shanghai, China). The antibodies are listed in Supplementary Table 1.

Mouse Breeding and Husbandry

The Ethics Committee at Nanjing University approved all animal studies. The male Rab8a$^{f/f}$ mice (eight-week-old) were generated previously (11) and were back-crossed with C57BL6 mice for at least 8 generations before these experiments. The male Myf5-Cre mice (eight-week-old, C57BL6 background) were as previously described (18). Mice were housed under a 12-h light/12-h dark cycle and were given free access to food and water unless stated otherwise.

Blood Chemistry

Blood glucose levels were determined using a Breeze-2 glucometer (Bayer). Serum free fatty acids (FFAs), triglycerides (TGs), and total cholesterol (TC) were measured as previously described (19).

Oral Glucose Tolerance Test and Insulin Tolerance Test

Mice were deprived of food overnight (16 h) for the oral glucose tolerance test or for 4 h for the insulin tolerance test. For the oral glucose tolerance test, a bolus of glucose (1.5 mg/g) was administered to the mice via oral gavage. For the insulin tolerance test, insulin (0.75 mU/g) was intraperitoneally injected into mice. Blood glucose levels were determined through blood taken from the tail.

Body Composition Analysis

Mice were anesthetized with isoflurane and body composition was measured with DEXA using a Lunar PIXImus-II densitometer (GE Healthcare). Images taken with the PIXImus-II densitometer were analyzed using PIXImus-II software.

Measurement of Liver TGs and TC

Liver TGs were measured as previously described (19). To measure liver TC, lipids were extracted with a chloroform-isopropanol-NP-40 (7:11:0.1) solution, and TC was measured after the organic solvent was removed using a LabAssay Cholesterol kit (catalog no. 294–65801; Wako Chemicals USA, Inc.).

Cell Culture and Transfection

Rat L6 myoblasts were obtained from the Cell Resource Center, Chinese Academy of Medical Sciences (Beijing, China) and maintained in medium containing 10% (v/v) fetal bovine serum. Lipofectamine-mediated transfection of L6 myoblasts was carried out as previously described (20). Rab8a siRNA (5′-GGAATAAGTGTGATGTGAA-3′, synthesized by Gene Pharma [Shanghai, China]) used for knockdown experiments is as previously described (17).

Measurement of LD Sizes and Neutral Lipid Exchange Rate

The sizes of the largest LDs and the lipid exchange rates in L6 myoblasts were measured as previously described (17).

Muscle Incubation and Glucose Uptake Ex Vivo

The soleus or extensor digitorum longus (EDL) muscle was isolated and subjected to stimulation with or without insulin. Muscle glucose was taken up as previously described (21).

Muscle Lipid Uptake and Oxidation Ex Vivo

Muscle lipid uptake and oxidation were measured as previously described (22), with modifications. Briefly, isolated soleus muscles were stimulated with or without insulin for 30 min, then incubated in Krebs-Ringer bicarbonate buffer (with or without insulin) containing ^{14}C-palmitic acid for 50 min. Upon the completion of incubation, the muscles were blotted dry and lysed in order to measure the radioisotopes within them using a Tri-Carb 2800TR scintillation counter. Gaseous $^{14}CO_2$ was evolved from the incubation media with 0.6 mol/L perchloric acid and trapped in benzethonium hydroxide–soaked filters. Radioactivity in trapped $^{14}CO_2$ was measured and used to determine muscle lipid oxidation. The sum of radioactivity in the muscle and gaseous $^{14}CO_2$ was used to calculate lipid uptake rates in muscle.

Biotinylation of Membrane Proteins

Cell surface proteins were biotinylated as previously described (23), with modifications. Briefly, isolated soleus muscles were stimulated with or without insulin for 50 min, then incubated in Krebs-Ringer bicarbonate buffer (with or without insulin) containing Sulfo-NHS-SS-Biotin (Thermo Fisher Scientific) for 30 min. Biotinylated surface proteins were precipitated from lysates using NeutrAvidin-Agarose (Thermo Fisher Scientific), and surface levels of GLUT4 and CD36 were determined by Western blotting using the respective antibodies.

Tissue Lysis, Subcellular Fractionation of the Brown Adipose Tissue, and Immunoblotting

Mouse tissues were harvested, homogenized, and analyzed via immunoblotting as previously described (21). Subcellular fractionation of the brown adipose tissue (BAT) was performed as previously described (21).

Real-time Quantitative PCR

Real-time quantitative PCR was performed using a StepOnePlus system (Applied Biosystems) and the primers listed in Supplementary Table 2 in order to measure the expression of target genes.

Immunofluorescence Staining and Imaging

Immunofluorescence staining was performed as previously described (20). Briefly, frozen tissue sections or single muscle fibers fixed in paraformaldehyde were sequentially incubated with primary antibodies and secondary antibodies conjugated with Alexa Fluor or Cy3/Cy5. As for BODIPY staining, frozen tissue sections or single muscle fibers were incubated with BODIPY 493/503. After incubation with antibodies or BODIPY, slides were mounted and photographed with a Leica or Olympus confocal microscope.

Statistical Analysis

Data are given as means ± SDs. Comparisons were made using the *t* test for two groups or two-way ANOVA for multiple groups using Prism software (GraphPad Software, Inc., San Diego, CA).

RESULTS

Deletion of Rab8a in the Myf5 Lineage Caused Hyperlipidemia and Exacerbated Obesity and Hepatic Steatosis in HFD-Fed Mice

Skeletal muscle cells originate from Myf5-lineage progenitors. We mated Rab8a$^{f/f}$ mice (11) with Myf5-Cre mice (18) to delete Rab8a in Myf5 lineage–derived tissues, including skeletal muscle, in the resultant Rab8a$^{f/f}$/Myf5-Cre mice (referred to here as Rab8a-mKO) (Supplementary Fig. 1). As expected, Rab8a expression was diminished in Myf5 lineage–derived tissues, including skeletal muscle and BAT, of Rab8a-mKO mice but not in other tissues analyzed (Fig. 1*A*). No apparent compensation was observed for expression of the related Rab8b, Rab10, and Rab13 in skeletal muscle of Rab8a-mKO mice (Supplementary Fig. 2*A*–*C*). When mice were fed a chow diet, neither body weight nor composition were distinguishable between the Rab8a-mKO and Rab8a$^{f/f}$ mice (Fig. 1*B* and *C* and Supplementary Fig. 3*A*–*C*). No difference was observed for blood glucose between the two genotypes in mice either fed ad libitum or fasted overnight (Fig. 1*E* and Supplementary Fig. 4). Plasma FFAs, TGs, and TC were also unaltered in the Rab8a-mKO mice under conditions of ad libitum feeding (Supplementary Fig. 4). However, plasma FFA and TG levels were significantly higher in the Rab8a-mKO mice than in the Rab8a$^{f/f}$ controls after an overnight fast (Fig. 1*E*). When fed an HFD, the Rab8a-mKO mice were heavier and contained more fat than the controls, but they had normal lean mass (Fig. 1*B* and *D* and Supplementary Fig. 3*D* and *E*). Similar to when fed a chow diet, after an overnight fast the Rab8a-mKO mice had normal blood glucose but higher levels of plasma FFAs, TGs, and TC than the controls eating an HFD (Fig. 1*F*). In addition to a phenotype of hyperlipidemia and obesity, the Rab8a-mKO mice had heavier livers and developed hepatosteatosis (Fig. 1*G*–*I*). Their livers had larger LDs (Supplementary Fig. 5*A* and *B*) and contained more TGs and TC than those of the controls (Fig. 1*H* and *I*).

Insulin-Stimulated Glucose Uptake Was Normal in Rab8a-Deficient Skeletal Muscle

Because Rab8a has been implicated in regulating GLUT4 trafficking in L6 muscle cells (12), we investigated whether its deletion in skeletal muscle could inhibit insulin-stimulated glucose uptake, which might indirectly affect lipid metabolism. We found that the insulin signaling pathway remained intact in Rab8a-deficient skeletal muscle, as evidenced by normal phosphorylation of protein kinase B (PKB), AS160, and glycogen synthase kinase 3 (Fig. 2*A* and *B* and Supplementary Fig. 6*A* and *B*). GLUT4 protein expression was also normal in Rab8a-deficient muscle (Fig. 2*C* and *D*). We then examined insulin-stimulated GLUT4 translocation in soleus muscles and found no difference between the two genotypes (Fig. 2*C* and *E* and Supplementary Fig. 6*C*). In agreement with the unaltered GLUT4 translocation, insulin-stimulated glucose uptake remained intact in both soleus and EDL muscles from the Rab8a-mKO mice (Fig. 2*F* and *G*). Furthermore, the Rab8a-mKO mice displayed normal glucose tolerance and insulin sensitivity (Supplementary Fig. 6*D* and *F*), and their insulin secretion remained normal upon glucose challenge (Supplementary Fig. 6*E*). These data show that Rab8a does not play an important role in regulating insulin-stimulated glucose uptake in skeletal muscle, and the hyperlipidemia and hepatosteatosis of the Rab8a-mKO mice was not due to an alteration in muscle glucose uptake.

Muscle LCFA Uptake Was Decreased in Rab8a-mKO Mice as a Result of Impaired CD36 Translocation and Expression

Discovery of the hyperlipidemia phenotype prompted us to investigate whether muscle lipid metabolism was impaired in the Rab8a-mKO mice. As expected, LCFA uptake was increased more than twofold in wild-type soleus muscles in response to insulin (Fig. 3*A*). By contrast, insulin could no longer stimulate LCFA uptake in Rab8a-deficient muscle (Fig. 3*A*). As a consequence, fatty acid oxidation was elevated more than twofold in response to insulin in wild-type soleus muscles; however, this insulin response was blunted in Rab8a-deficient muscle (Fig. 3*B*). In agreement with their defective LCFA uptake in muscle, the Rab8a-mKO mice were unable to efficiently clear lipids in the blood after an oral lipid load when compared with their Rab8a$^{f/f}$ littermates (Fig. 3*C* and *D*). Hepatic output of TGs through secretion of TG-rich VLDL might also contribute to hyperlipidemia in the Rab8a-mKO mice. To address this possibility, we treated mice with an inhibitor tyloxapol targeting lipoprotein lipase (LPL) that is a key enzyme in hydrolyzing TGs in VLDL to release FFA for absorption by skeletal muscle. Tyloxapol significantly elevated blood TGs in the Rab8a$^{f/f}$ mice but failed to exert such an effect in the Rab8a-mKO mice within 2 h after administration (Fig. 3*E*). These data demonstrate that impaired lipid uptake in muscle but not hepatic VLDL secretion most likely underlies the hyperlipidemia phenotype in the Rab8a-mKO mice.

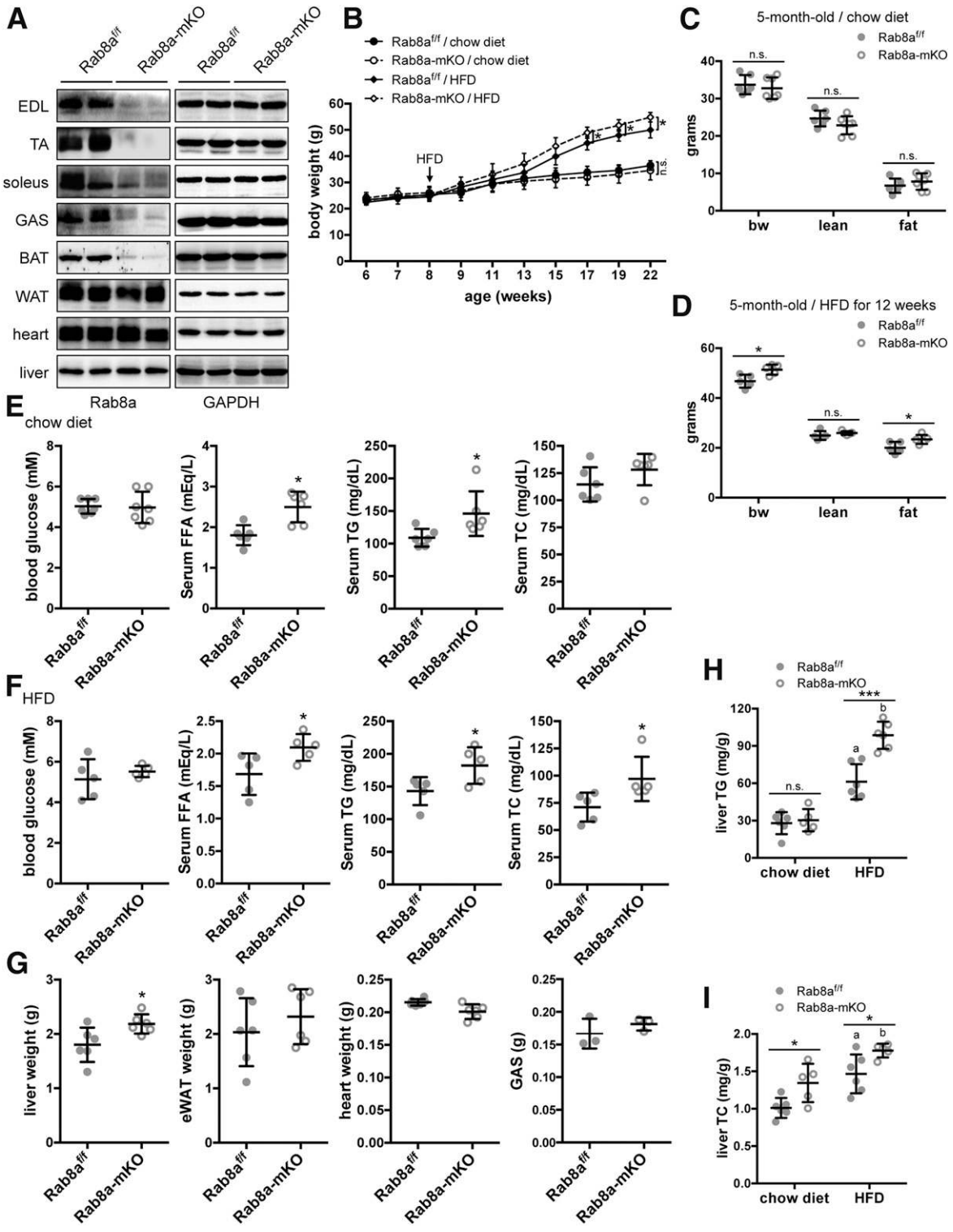

Figure 1—Body growth, body composition, and whole-body lipid metabolism in the Rab8a-mKO mice consuming a chow diet or an HFD. *A*: Expression of Rab8a in various tissues of the Rab8a-mKO mice, with GAPDH as the loading control. The Rab8a-mKO mice and their wild-type Rab8a$^{f/f}$ littermate controls were obtained by mating Rab8a$^{f/f}$ mice with Rab8a$^{f/f}$/Myf5-Cre mice. *B*: Body weights of the male Rab8a$^{f/f}$ and Rab8a-mKO mice eating a chow diet or an HFD (n = 5–8). *C* and *D*: Body composition of the male Rab8a$^{f/f}$ and Rab8a-mKO mice consuming a chow diet (*C*) or an HFD (*D*), measured at 5 months of age (n = 5–8). *E* and *F*: FFA, TG, and TC levels in the serum of male Rab8a$^{f/f}$ and Rab8a-mKO mice consuming a chow diet (*E*) or an HFD (*F*) but fasted overnight, measured at the age of 5 months (n = 5–6). *G*: Weight of tissues from the male Rab8a$^{f/f}$ and Rab8a-mKO mice consuming an HFD, measured at the age of 6 months (n = 6). *H* and *I*: TG (*H*) and TC (*I*) content in the livers of the male Rab8a$^{f/f}$ and Rab8a-mKO mice fed a chow diet or an HFD, measured at the age of 6 months (n = 5–6). Statistical analyses were performed with the *t* test (*B*–*G*) or two-way ANOVA (*H* and *I*). $^{*}P < 0.05$; $^{***}P < 0.001$. $^{a}P < 0.001$ (Rab8a$^{f/f}$ HFD vs. chow diet). $^{b}P < 0.01$ (Rab8a-mKO HFD vs. chow diet). eWAT, epididymal white adipose tissue; GAS, gastrocnemius; n.s., not significant; TA, tibialis anterior.

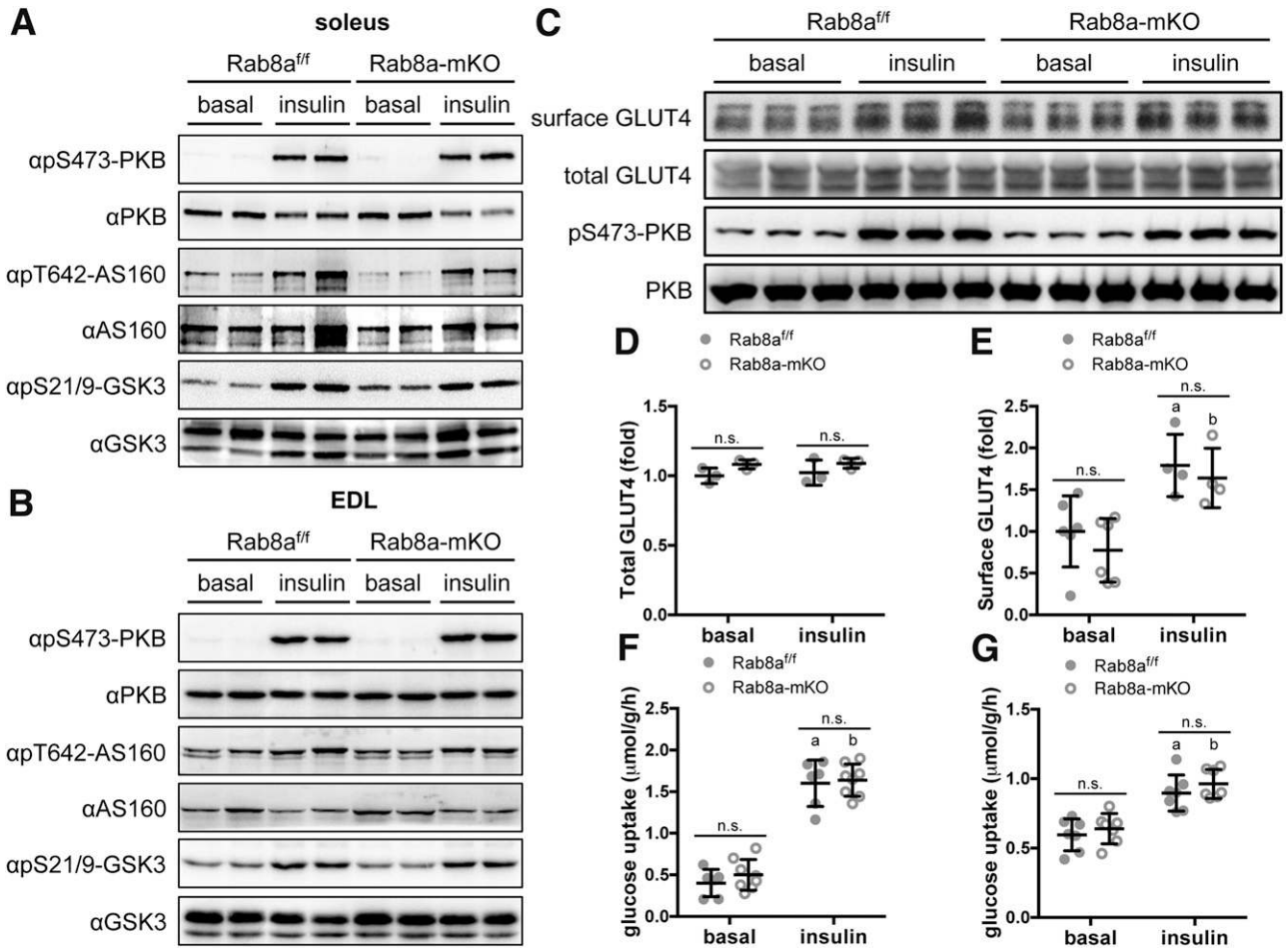

Figure 2—Muscle GLUT4 translocation and glucose uptake in Rab8a-mKO mice. *A* and *B*: Insulin signaling in soleus (*A*) or EDL (*B*) muscles of the Rab8a$^{f/f}$ and Rab8a-mKO mice, either intraperitoneally injected with insulin or not receiving an injection. *C*: Representative blots for measurements of total and surface GLUT4 in ex vivo soleus muscle stimulated by insulin or not. Cell-surface GLUT4 was biotinylated and isolated using NeutrAvindin-Agarose. *D* and *E*: Quantitative data for total (*D*) and surface (*E*) GLUT4 in ex vivo soleus muscle stimulated with insulin or not (n = 3–6). $^{a}P < 0.05$, Rab8a$^{f/f}$ insulin vs. basal; $^{b}P < 0.05$, Rab8a-mKO insulin vs. basal. *F* and *G*: Glucose uptake in isolated soleus (*F*) or EDL (*G*) muscles of the male Rab8a$^{f/f}$ and Rab8a-mKO mice (n = 6–8). $^{a}P < 0.001$, Rab8a$^{f/f}$ insulin vs. basal; $^{b}P < 0.001$, Rab8a-mKO insulin vs. basal. Statistical analyses for *D*–*G* were carried out using two-way ANOVA. n.s., not significant.

Lipid uptake in muscle has been reported to be mainly mediated by CD36, which undergoes translocation in response to insulin in skeletal muscle (3). We found that Rab8a partially colocalized with CD36 in skeletal muscle (Fig. 3*F*). When Rab8a was knocked down in L6 myotubes, it did not affect expression of CD36 but impaired insulin-stimulated CD36 translocation (Fig. 3*G*). Insulin increased more than twofold CD36 levels at the cell surface in wild-type skeletal muscle. However, insulin-stimulated CD36 translocation was significantly inhibited in Rab8a-deficient muscle, despite its normal expression in these young (3-month-old) Rab8a-mKO mice (Fig. 3*H*–*J*). Interestingly, muscle CD36 protein levels were markedly decreased in older (6-month-old) Rab8a-mKO mice compared with their Rab8a$^{f/f}$ littermate controls, despite normal mRNA levels in skeletal muscle from these mice fed a chow diet (Fig. 4*A* and *B*). When mice were transferred from chow to an HFD, CD36 mRNA levels increased in the Rab8a$^{f/f}$ muscle but remained largely unchanged in the Rab8a-deficient muscle (Fig. 4*B*). Moreover, CD36 protein levels were still lower in skeletal muscle from the Rab8a-mKO mice eating an HFD (Fig. 4*C* and *D*). In contrast to CD36, two other membrane proteins—namely, GLUT4 and transferrin receptor—were not altered in Rab8a-deficient skeletal muscle (Fig. 4*C*). Interestingly, we found that LPL expression was significantly decreased in Rab8a-deficient skeletal muscle at both the mRNA and protein levels (Fig. 4*B* and *C*). Diminution of LPL suggested that degradation of TGs from VLDL might be impaired. In agreement with this, more TGs were detected in the VLDL fractions from the Rab8a-mKO mice (Supplementary Fig. 7). LPL is a target gene of peroxisome proliferator–activated receptor α (PPARα) (24,25), whose expression was normal in skeletal muscle from Rab8a-mKO mice (Fig. 4*B* and *C*). Fatty acids are ligands for PPARα, and CD36 is a known regulator of PPARα through ligand activation (26). Decreased uptake of lipids into skeletal muscle

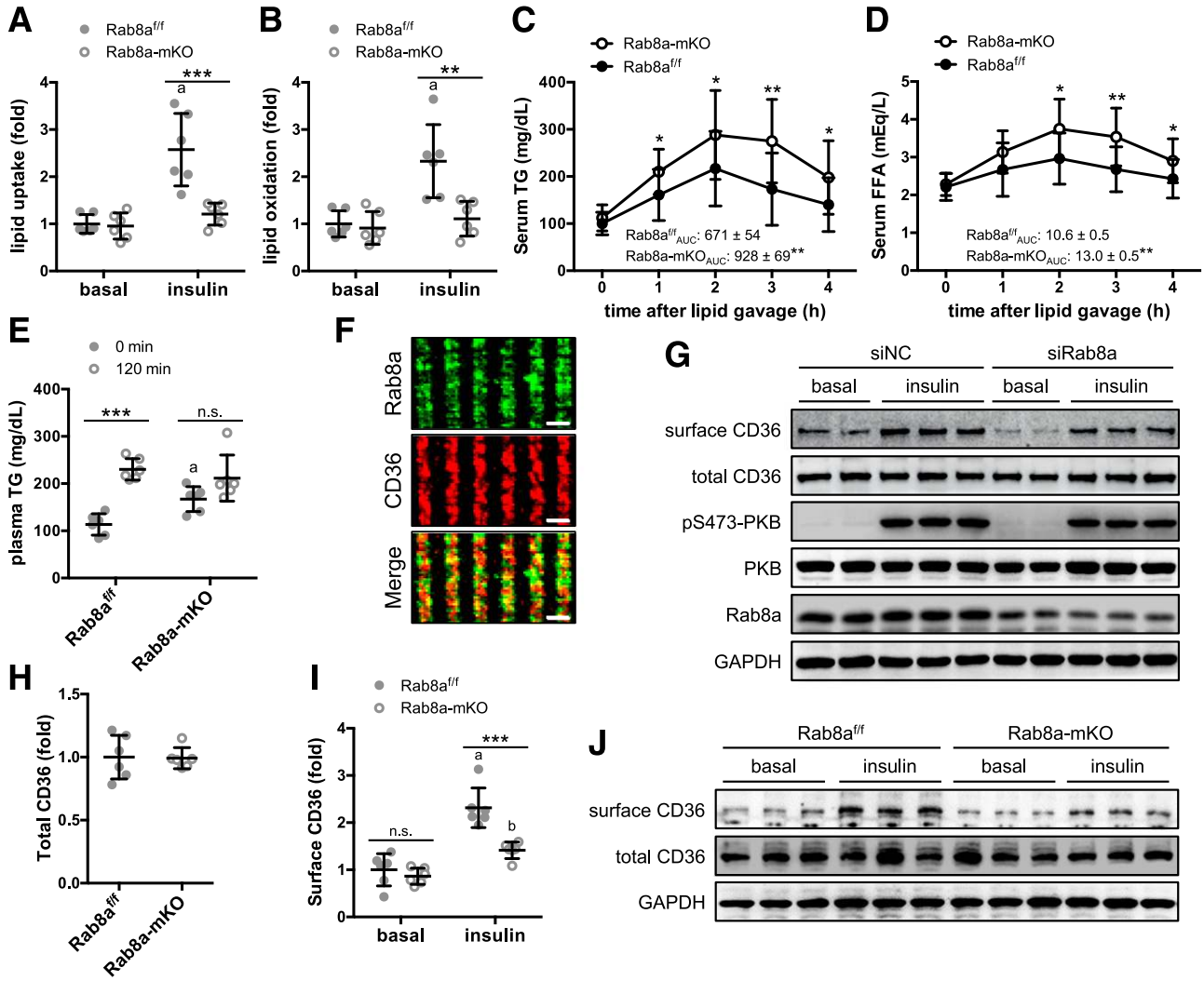

Figure 3—Muscle CD36 translocation and lipid metabolism in the Rab8a-mKO mice. *A* and *B*: Lipid uptake (*A*) and oxidation (*B*) in isolated soleus muscles of the male Rab8a$^{f/f}$ and Rab8a-mKO mice (n = 6). $^{**}P < 0.01$; $^{***}P < 0.001$. $^{a}P < 0.001$ (Rab8a$^{f/f}$ insulin vs. basal). *C* and *D*: Serum levels of TGs (*C*) and FFAs (*D*) after lipid administration. Mice were deprived of food for 4 h and administered olive oil (6 μL/g body weight) via oral gavage. Blood was collected via a tail bleed at the indicated time points and was used to measure serum TGs and FFAs (n = 13–14). $^{*}P < 0.05$; $^{**}P < 0.01$. *E*: Plasma TG levels upon tyloxapol administration. Mice were fasted overnight and administered tyloxapol (200 mg/kg) via intraperitoneal injection. Plasma TG levels were determined before and 120 min after tyloxapol administration (n = 6). $^{***}P < 0.001$. $^{a}P < 0.05$, Rab8a-mKO basal vs. Rab8a$^{f/f}$ basal. n.s., not significant. *F*: Subcellular localization of Rab8a and CD36 in mouse muscle fibers. Scale bars = 2 μm. *G*: Cell-surface CD36 levels in L6 myotubes upon downregulation of Rab8a. Rab8a was knocked down via siRNA in L6 myotubes that were stimulated with or without 100 nmol/L insulin. Cell-surface CD36 was biotinylated and isolated using NeutrAvindin-Agarose. siNC, negative control siRNA. *H*–*J*: Cell-surface CD36 levels in isolated soleus muscles of the male Rab8a$^{f/f}$ and Rab8a-mKO mice (n = 6). Cell-surface CD36 was biotinylated and isolated using NeutrAvindin-Agarose. Quantitative data of total (*H*) and cell-surface (*I*) CD36. $^{***}P < 0.001$. $^{a}P < 0.001$ (Rab8a$^{f/f}$ insulin vs. basal). $^{b}P < 0.05$, Rab8a-mKO insulin vs. basal. n.s., not significant. *J*: Representative blots.

due to impaired CD36 translocation/expression might therefore reduce PPARα activity, which might consequently decrease LPL expression in Rab8a-deficient skeletal muscle.

Rab8a was also deleted in the BAT of Rab8a-mKO mice, but its deletion did not affect the expression of total or cell-surface CD36 in this tissue (Supplementary Fig. 8). Expression of key genes involved in lipid transport, lipogenesis, lipolysis, and β-oxidation were normal, but that of thermogenic genes was increased in the BAT of Rab8a-mKO mice (Supplementary Fig. 8*B*–*D*), suggesting that the thermogenic function of BAT might not be impaired in these mice. Furthermore, specific deletion of Rab8a in BAT and white adipose tissue (WAT) in the Rab8af/f/AdipoQ-Cre (Rab8a-aKO) mice did not cause hyperlipidemia and hepatosteatosis (Supplementary Fig. 9). These data suggest that Rab8a-deficiency in BAT was likely not responsible for the hyperlipidemia and hepatosteatosis phenotype in the Rab8a-mKO mice, although we cannot rule out the possibility that Rab8a deletion in the WAT might counteract possible effects from BAT in the Rab8a adipose-specific knockout mice.

Together, these data show that the entry of lipids into skeletal muscle was impaired in the Rab8a-mKO mice,

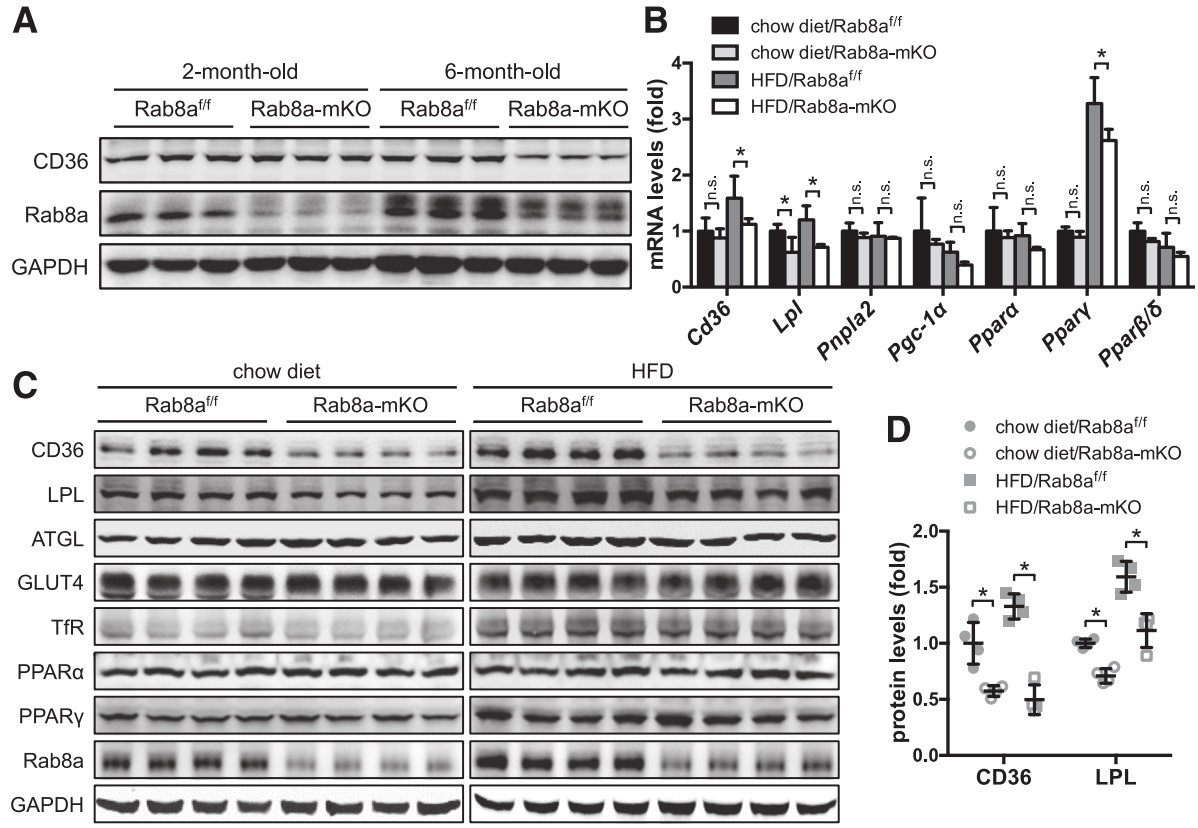

Figure 4—Expression of CD36 and LPL in skeletal muscle of Rab8a-mKO mice. *A*: CD36 protein levels in skeletal muscle of the male Rab8a$^{f/f}$ and Rab8a-mKO mice at different ages. *B*: mRNA expression of *Cd36*, *Lpl*, *Pnpla2*, *Pgc-1α*, *Pparα*, *Pparγ*, and *Pparβ/δ* in skeletal muscle of the Rab8a$^{f/f}$ and Rab8a-mKO mice eating a chow diet or an HFD at the age of 6 months (n = 4). *C*: Protein expression of CD36, LPL, ATGL, GLUT4, transferrin receptor (TfR), PPARα, and PPARγ in skeletal muscle of the male Rab8a$^{f/f}$ and Rab8a-mKO mice eating a chow diet or an HFD at the age of 6 months. *D*: Quantitation of CD36 and LPL protein levels in skeletal muscle of the male Rab8a$^{f/f}$ and Rab8a-mKO mice eating a chow diet or an HFD at the age of 6 months (n = 4). *P < 0.05. n.s., not significant.

probably because CD36 translocation was inhibited and CD36 expression was downregulated, which may explain the hyperlipidemia in these mice.

LD Fusion Was Impaired in Rab8a-Deficient Muscle Cells

A portion of lipids absorbed into skeletal muscle is temporally stored in LDs. When mice were fed an HFD, LDs became enlarged in skeletal muscle from the Rab8a$^{f/f}$ controls. Although LDs in Rab8a-deficient skeletal muscle still became enlarged, they were substantially smaller than those in control muscle under HFD conditions (Fig. 5*A* and *B*). Rab8a has been shown to regulate LD fusion in adipocytes (17). Therefore, in addition to impaired lipid uptake, defective LD fusion might be another underlying cause of the smaller LDs in Rab8a-deficient skeletal muscle. In agreement with this possibility, Rab8a partially colocalized with LDs within muscle fibers (Fig. 5*A* and *B*) and L6 cells (Supplementary Fig. 10*A* and *B*). We then used L6 cells to examine a possible role of Rab8a in regulating LD fusion in muscle cells. Interestingly, the sizes and lipid exchange rates of LDs were both significantly decreased when Rab8a was downregulated in L6 cells (Fig. 5*C–F* and Supplementary Fig. 10*C* and *D*), suggesting that Rab8a deficiency inhibits LD fusion in muscle cells. The Rab8a-mKO mice displayed normal expression of adipose triglyceride lipase (ATGL; an important lipase for lipolysis) at both the mRNA and protein levels, indicating that their lipolysis in skeletal muscle might be unaltered (Fig. 4*B* and *C*). Together, these data demonstrate that Rab8a deficiency decreases lipid storage in part through impairing LD fusion in muscle cells.

Hepatic Lipogenesis and Cholesterol Biosynthesis Were Enhanced in Rab8a-mKO Mice

To gain insights into how Rab8a deficiency in muscle exacerbated HFD-induced hepatosteatosis, we examined the expression of key genes in lipid metabolism in the liver. The mRNA levels of lipogenic genes such as *Acc1*, *Fasn*, and *Scd1*, and levels of FASN protein, were upregulated in the livers of Rab8a-mKO mice fed the chow diet and those fed the HFD (Fig. 6*A* and *D*), suggesting that hepatic lipogenesis was elevated in these mice. Moreover, mRNA expression of GPAT1, a key enzyme for hepatic triglyceride synthesis, was upregulated in the livers of Rab8a-mKO mice (Fig. 6*D*).

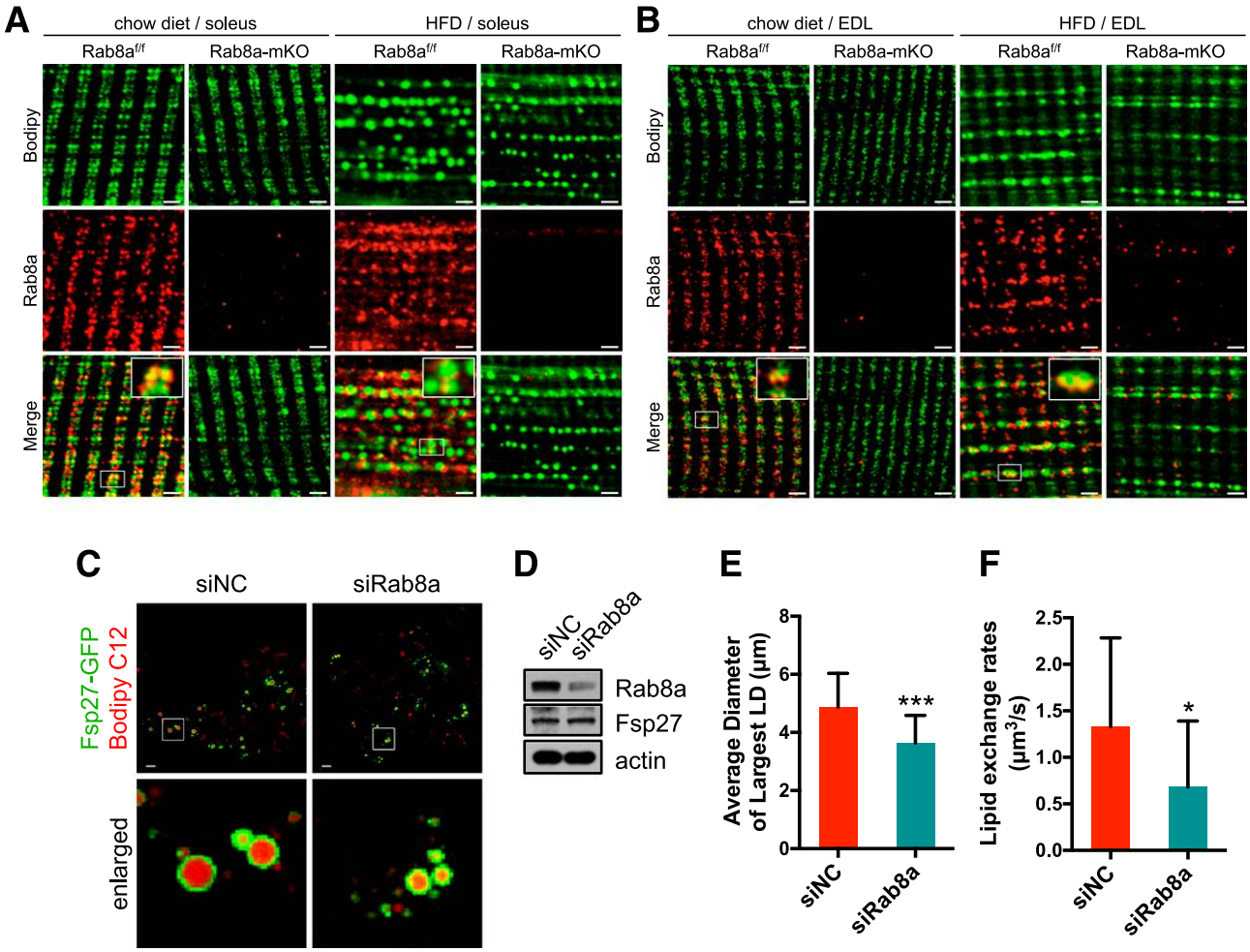

Figure 5—LD sizes and fusion in Rab8a-deficient muscle cells and skeletal muscle. *A* and *B*: BODIPY staining of LDs and Rab8a staining in soleus (*A*) and EDL (*B*) muscles of the male Rab8a$^{f/f}$ and Rab8a-mKO mice eating a chow diet or an HFD. Images were taken using an Olympus FV1000 microscope with a 60× oil objective lens. BODIPY and Cy3 were excited (for Rab8a detection) using the 488-nm and 559-nm laser beams, respectively. The light emitted for BODIPY was detected with a 500- to 545-nm band-pass filter, and Cy3 with a 570- to 670-nm band-pass filter. Images were processed using an Olympus FV10-ASW 1.7 Viewer. Insets show enlarged images of the outlined regions. Scale bars = 2 μm. *C*: Representative images of LDs in Rab8a-knockdown L6 myoblasts. Rat L6 myoblasts cotransfected with Fsp27 and indicated siRNAs were further treated with 200 μmol/L oleic acid complexed to albumin before being fixed and stained with BODIPY 493/503. Images were obtained using an LSM710 confocal microscope (Carl Zeiss). Scale bars = 10 μm. *D*: Rab8a and Fsp27 protein levels in L6 myoblasts transfected with Fsp27 and siRNAs. *E*: Quantitative data of the largest LD diameters in L6 myoblasts transfected with Fsp27 and siRNAs. The diameter of the largest LD in one cell was measured in at least 120 cells in each condition (n = 126 [siNC] and n = 171 [siRab8a]). ***P < 0.001. *F*: LD lipid exchange rates in L6 myoblasts transfected with Fsp27 and siRNAs. L6 myoblasts cotransfected with Fsp27 and siRNAs were further treated with 200 μmol/L oleic acid complexed to albumin and 1 μg/mL BODIPY 558/568 C12 fatty acid for 15 h. Cells were changed to fresh medium for 1 h before lipid exchange rates were measured using an LSM710 confocal microscope. Photo-bleaching was performed on selected LD pairs with 500 interactions at 100% laser power (543-nm diode laser), followed by time-lapse scanning with a 12.5-s interval. Mean optical intensities within LD core regions were measured simultaneously and calculated as the percentage of the original fluorescent intensity in order to obtain fluorescence recovery curves. About 20 pairs of LDs were measured in each condition (n = 20–22). *P < 0.05. Statistical analyses for *E* and *F* were carried out using the *t* test. siNC, negative control siRNA.

Similarly, cholesterol biosynthesis might also be increased in the livers of these mice, as evidenced by elevated mRNA levels of cholesterol biosynthetic genes such as *Hmgcs1*, *Hmgcr*, *Fdps*, *Cyp51a1*, and *Dhcr7* (Fig. 6*E*). Furthermore, expression of the LDL receptor was upregulated in the livers of Rab8a-mKO mice fed the chow diet and those fed the HFD (Fig. 6*A* and *E*). By contrast, hepatic expression of the key lipolytic enzymes PNPLA3 and ATGL, and key regulators of β-oxidation such as PPARα, ACADL, and CPT1, were all normal in the livers of Rab8a-mKO mice (Fig. 6*A* and *F*). Together, these data suggest that exacerbated hepatosteatosis in HFD-fed Rab8a-mKO mice was most likely due to enhanced lipogenesis, TG synthesis, and cholesterol biosynthesis in the livers of these animals.

In contrast to the liver, no significant alterations in the key genes involved in lipid metabolism were detected in the adipose tissue of Rab8a-mKO mice fed either the chow diet or the HFD (Supplementary Fig. 11*A* and *B*).

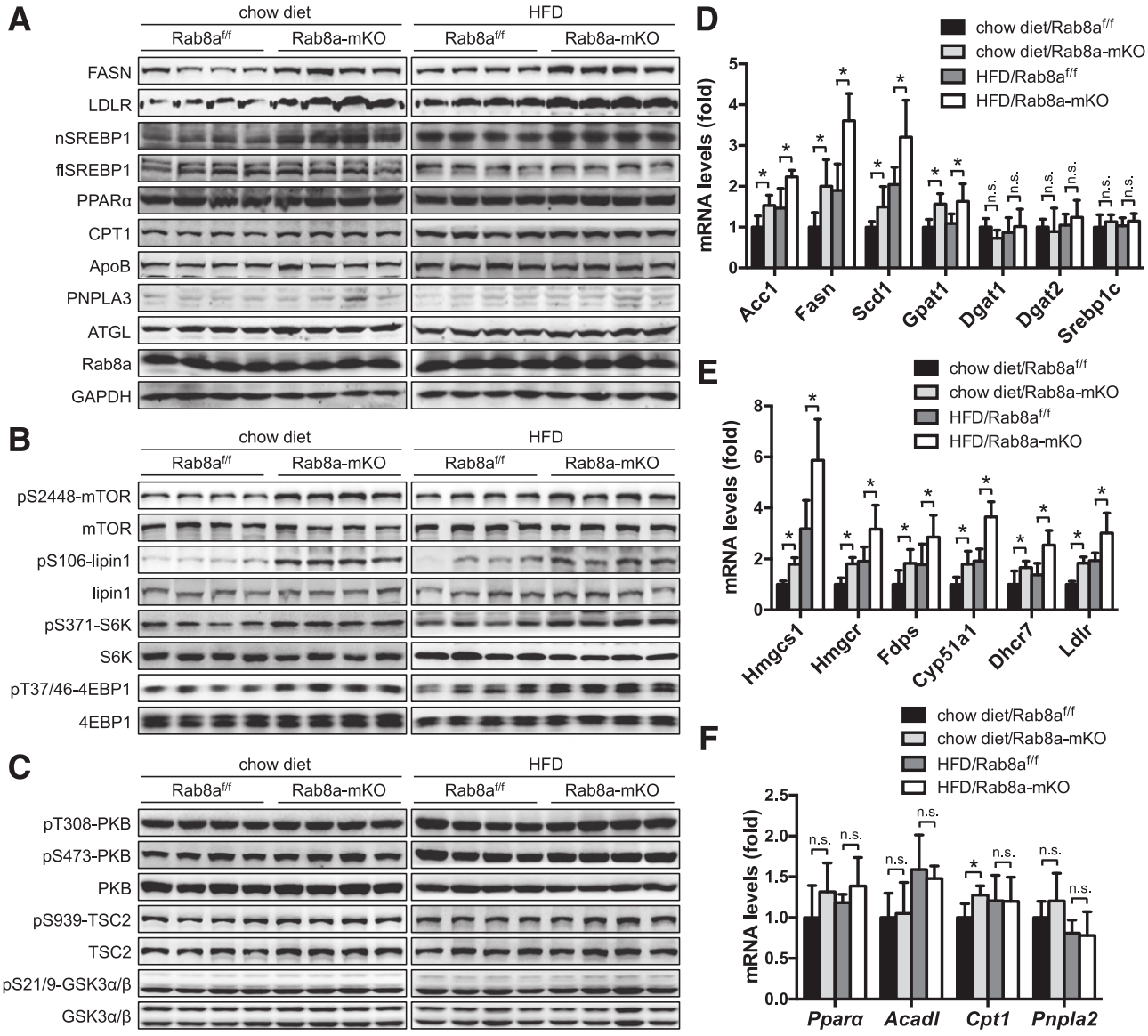

Figure 6—Expression of key genes in lipid metabolism and mTOR activation in the liver of Rab8a-mKO mice. *A–C*: Protein expression of key genes in lipid metabolism (*A*) and expression and phosphorylation of components of the mTOR (*B*) and PKB (*C*) pathways in the liver of male Rab8a$^{f/f}$ and Rab8a-mKO mice eating a chow diet or an HFD. *D–F*: mRNA expression of key genes in lipid metabolism in the liver of male Rab8a$^{f/f}$ and Rab8a-mKO mice eating a chow diet or an HFD (n = 5–6). Statistical analyses were carried out using two-way ANOVA. *$P < 0.05$. flSREBP1, full-length SREBP1; n.s., not significant; nSREBP1, cleaved nuclear SREBP1.

Activation of the Mammalian Target of Rapamycin Pathway Enhanced Hepatic Lipogenesis and Cholesterol Biosynthesis in Rab8a-mKO Mice

We next sought to find potential mechanisms for enhanced hepatic lipogenesis and cholesterol biosynthesis in the Rab8a-mKO mice. SREBP1 is a common regulator of the above-mentioned lipogenic genes (27,28); its mRNA and full-length protein levels were normal in the livers of Rab8a-mKO mice (Fig. 6*A* and *B*). Full-length SREBP1 resides on the endoplasmic reticulum, where its N-terminal portion can be cleaved and thereafter translocated into the nucleus to regulate transcription of lipogenic genes. Importantly, the cleaved nuclear form of SREBP1 was increased in the livers of Rab8a-mKO mice despite normal expression of full-length SREBP1 (Fig. 6*A*). Consistent with the cleavage of SREBP1 being under the control of the mammalian target of rapamycin (mTOR) (29,30), mTOR activation—as evidenced by its own phosphorylation and the phosphorylation of its substrates, S6K and 4EBP1—was increased in the livers of Rab8a-mKO mice fed a chow diet and those fed an HFD (Fig. 6*B*). The activity of SREBP1 in the nucleus is inhibited by lipin1, whose phosphorylation by mTOR prevents its entry into the nucleus (31). Consistent with mTOR activation, phosphorylation of lipin1 was elevated in the livers of Rab8a-mKO mice (Fig. 6*B*), which indicates a higher activity of SREBP1 in the nucleus. Activation of mTOR was not due

to the upstream regulators PKB and TSC2, because their phosphorylation remained normal in the livers of Rab8a-mKO mice (Fig. 6*C*). To establish a causal relationship between mTOR activation and upregulation of hepatic lipogenesis and cholesterol biosynthesis, we treated the Rab8a-mKO and Rab8a$^{f/f}$ mice with the mTOR inhibitor rapamycin. Rapamycin decreased phosphorylation of mTOR and lipin1, and normalized nuclear SREBP1 levels in the livers of Rab8a-mKO mice (Fig. 7*A*). Consequently, expression of lipogenic and cholesterol biosynthetic genes was normalized in the rapamycin-treated livers of Rab8a-mKO mice (Fig. 7*B*), which further confirmed that increased expression of lipogenic genes in the livers of Rab8a-mKO mice was due to mTOR activation. Importantly, rapamycin treatment normalized TC levels in the livers of Rab8a-mKO mice (Fig. 7*D*). Lipids have been shown to activate mTOR (32,33); this led us to speculate

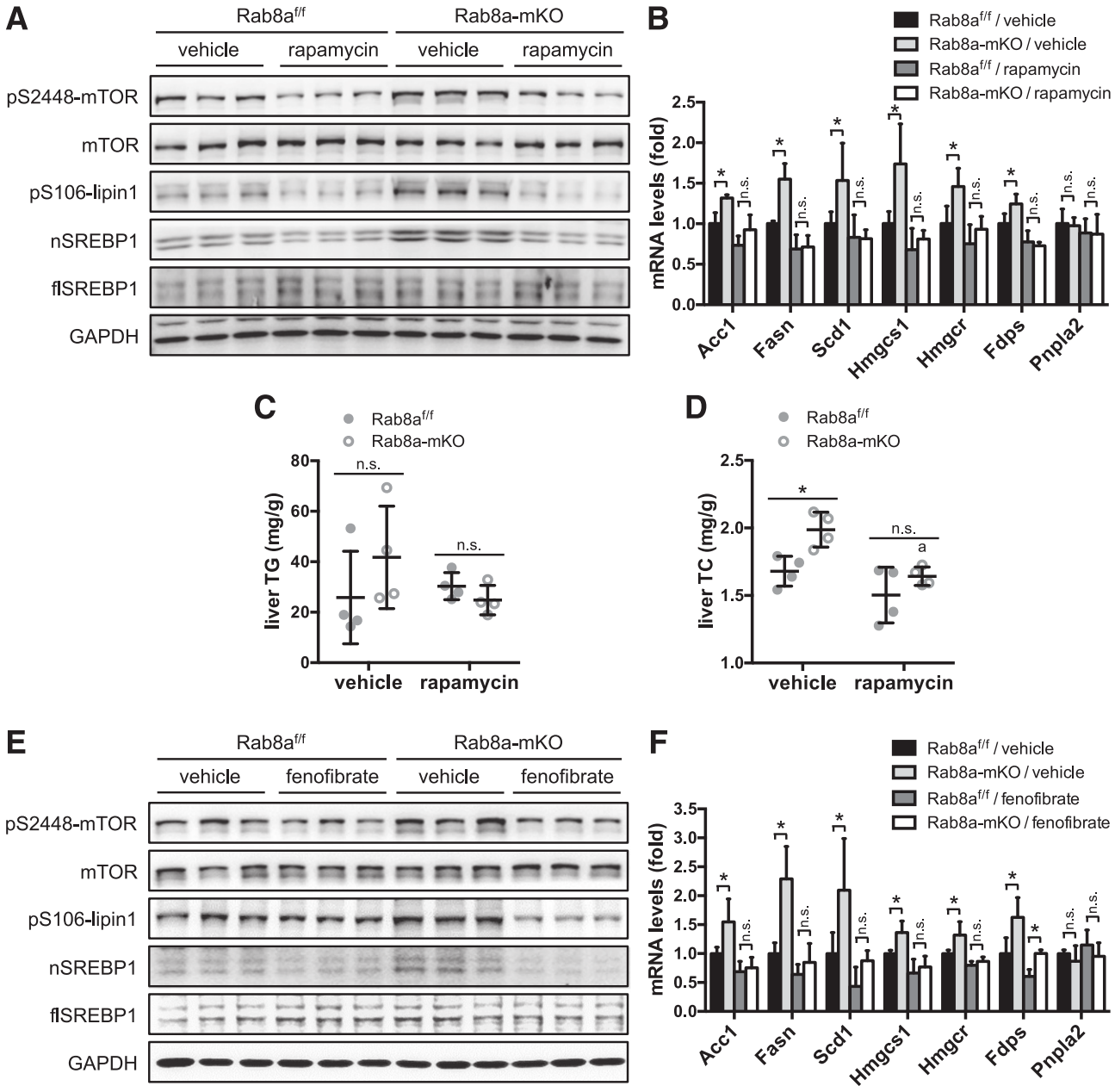

Figure 7—Expression of key genes in lipid metabolism and mTOR activation in the liver of the Rab8a-mKO mice upon treatment with rapamycin or fenofibrate. *A* and *B*: The mTOR-lipin1-SREBP1 pathway (*A*) and mRNA expression of key genes in lipid metabolism (*B*) in the livers of female Rab8a$^{f/f}$ and Rab8a-mKO mice intraperitoneally injected with rapamycin (1 mg/kg) or vehicle (0.2% microcrystalline cellulose plus 0.25% Tween-80 in water) for 8 days (n = 4). *C* and *D*: TGs (*C*) and TC (*D*) in the livers of female Rab8a$^{f/f}$ and Rab8a-mKO mice intraperitoneally injected with rapamycin or vehicle for 8 days (n = 4). $^{a}P < 0.05$, Rab8a-mKO rapamycin vs. vehicle. *E*: The mTOR-lipin1-SREBP1 pathway in the liver of female Rab8a$^{f/f}$ and Rab8a-mKO mice gavaged with fenofibrate (25 mg/kg) or vehicle (water) for 8 days. *F*: mRNA expression of key genes in lipid metabolism in the liver of female Rab8a$^{f/f}$ and Rab8a-mKO mice gavaged with fenofibrate or vehicle for 8 days (n = 4–6). Statistical analyses were carried out using two-way ANOVA. $^{*}P < 0.05$. flSREBP1, full-length SREBP1; n.s., not significant; nSREBP1, cleaved nuclear SREBP1.

that hyperlipidemia might underlie mTOR activation in the livers of Rab8a-mKO mice. Treatment with the lipid-lowering drug fenofibrate significantly decreased serum FFAs, TGs, and TC in these mice (Supplementary Fig. 12). Indeed, treatment with fenofibrate attenuated activation of the mTOR-lipin1 pathway and reduced the hepatic expression of lipogenic and cholesterol biosynthetic genes in the Rab8a-mKO mice (Fig. 7*E* and *F*). Together, these data show that elevated serum lipid levels might activate the mTOR-lipin1-SREBP1 pathway, consequently enhancing lipogenesis and cholesterol biosynthesis in the livers of Rab8a-mKO mice.

In agreement with the unaltered expression of key genes of lipid metabolism in adipose tissue (Supplementary Fig. 11*A*), the mTOR-lipin1 pathway remained normal in this tissue from Rab8a-mKO mice (Supplementary Fig. 11*B*).

DISCUSSION

In this study we show that Rab8a regulates lipid uptake and LD fusion in skeletal muscle. Its deficiency in skeletal muscle impairs lipid uptake and storage in muscle; it also causes hyperlipidemia and exacerbates HFD-induced hepatosteatosis by promoting lipogenesis and cholesterol biosynthesis in the liver (Fig. 8). Our findings shed light on a new role for skeletal muscle in the pathogenesis of hyperlipidemia and NAFLD.

Rab8a has been implicated in regulating various membrane trafficking processes, including GLUT4 trafficking (12) and CD36 trafficking (14). The majority of published studies were carried out using culture cell lines, and the in vivo functions of Rab8a have only been studied in small intestine using Rab8a knockout mice (11). Despite the importance of Rab8a in regulating GLUT4 trafficking in L6 muscle cells (12), our in vivo studies show that it was dispensable for glucose uptake in mouse skeletal muscle. It is currently not clear whether compensatory responses are available to regulate GLUT4 translocation and glucose uptake in Rab8a-deficient skeletal muscle. In agreement with a role in regulating CD36 trafficking in HL-1 cardiomyocytes (14), Rab8a was required for insulin-stimulated CD36 translocation in mouse skeletal muscle. CD36 translocation was regulated by Rab8a in a tissue-dependent manner. Deletion of Rab8a impaired insulin-stimulated CD36 translocation in skeletal muscle but not in BAT. Nevertheless, Rab8a deletion in BAT might contribute to some of the phenotypes observed in the Rab8a-mKO mice through yet-unidentified mechanisms. We note that Rab8a was also indispensable for maintaining CD36 protein levels in older mice. Rab8a deficiency has been shown to cause mislocalization of apical peptidases and transporters to the lysosome for degradation, consequently decreasing their protein levels in small intestine and interfering with nutrient absorption (11). Ubiquitination of CD36 has also been reported to serve as a sorting signal for its lysosomal degradation after being internalized into early/sorting endosomes (34). One possibility is that this ubiquitination-dependent pathway for lysosomal degradation of CD36 might be chronically activated in Rab8a-deficient skeletal muscle, which might decrease CD36 proteins in older mice. This chronic CD36 degradation signal might be absent in the acute Rab8a-knockdown culture

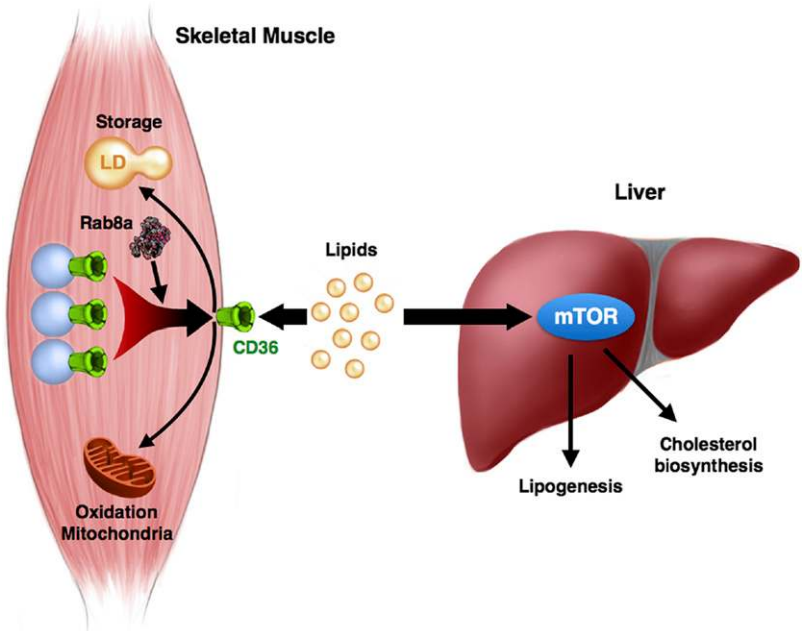

Figure 8—A model for muscle-liver communication in the control of lipid homeostasis. Rab8a regulates lipid uptake through CD36 translocation and lipid storage via LD fusion in skeletal muscle. Its deficiency in skeletal muscle impairs lipid uptake and storage in muscle and leads to hyperlipidemia, which activates the mTOR-SREBP1 pathway in the liver. Consequently, hepatic lipogenesis and cholesterol biosynthesis are increased, which results in hepatosteatosis.

cell system because of either its possible time-dependent nature or its potential non-cell-autonomous origin.

LDs are important organelles for lipid storage in many tissues, including skeletal muscle and adipose tissues (7). Despite the different sizes of the LDs in these two tissues, our studies demonstrate that LD fusion requires Rab8a as a common regulator in both skeletal muscle and adipose tissues (as seen in this study and as described in ref. 17). Our data also show that lipid storage through LD fusion might be coordinated with lipid uptake in skeletal muscle, and Rab8a was involved in both processes. Fatty acids and their derivatives can cause lipotoxicity to skeletal muscle, and their conversion into TGs can facilitate detoxification of fatty acids (6). We suspect that the possible coordination between lipid uptake and storage via Rab8a might help to reduce lipotoxicity in skeletal muscle.

Our study demonstrates the importance of skeletal muscle in the regulation of whole-body lipid homeostasis through communication with lipogenic and cholesterol biosynthetic pathways in the liver. The interaction between muscle and liver storage of lipids is not a simple process of substrate redistribution from the muscle into the liver. Rather, it is cross talk between these two organs involving induction of lipogenic and cholesterol biosynthetic genes in the liver through the mTOR-lipin1-SREBP1 pathway. Although our data suggest serum lipids are important mediators in the regulation of hepatic mTOR activation in Rab8a-mKO mice, some other skeletal muscle–derived factors might also contribute to this activation. Physical inactivity is one of the underlying causes of NAFLD (35), and exercise is an effective treatment to combat NAFLD and can reduce the amount of liver fat in the absence of significant weight loss (36,37). The mechanisms by which exercise decreases liver fat are not fully understood, although multiple pathways may conceivably be involved. Interestingly, exercise can increase the lipid content of skeletal muscle (38). Therefore, whether the organ cross talk between skeletal muscle and liver identified in this study may contribute to the therapeutic effects of exercise on NAFLD is an intriguing question that deserves further investigation in the future.

In summary, our findings demonstrate that Rab8a is an important molecule regulating both lipid uptake and LD fusion in skeletal muscle. Lipid entry into skeletal muscle for subsequent metabolism or storage is important for whole-body lipid homeostasis, and its impairment causes hyperlipidemia and promotes NAFLD.

Acknowledgments. The authors thank Carol MacKintosh (University of Dundee, U.K.) for proofreading the manuscript and Yanqiu Ji (Model Animal Research Center, Nanjing University, China) for assistance with genotyping of mice.

Funding. Financial support was provided by the Ministry of Science and Technology of China (grant nos. 2014CB964704 and 2014BAI02B01 [National Key Scientific Research Program of China] and 2014AA021104 [the National High Technology Research and Development Program of China]), the National Natural Science Foundation of China (grant nos. 31571211 and 31671456), and the Ministry of Education of China (grant nos. 20120091120048 and NCET-13-0270).

Duality of Interest. No potential conflicts of interest relevant to this article were reported.

Author Contributions. Q.C., P.R., D.X., S.Z., L.C., B.X., Q.D., C.Q., and Y.S. performed experiments, analyzed data, and reviewed and edited the manuscript. T.-J.Z. and P.L. reviewed and edited the manuscript. H.Y.W. and S.C. designed the experiments, analyzed data, and wrote the manuscript. All authors approved the final version of the manuscript. S.C. is the guarantor of this work and, as such, had full access to all the data in the study and takes responsibility for the integrity of the data and the accuracy of the data analysis.

References

1. Katz LD, Glickman MG, Rapoport S, Ferrannini E, DeFronzo RA. Splanchnic and peripheral disposal of oral glucose in man. Diabetes 1983;32:675–679
2. Stöckli J, Fazakerley DJ, James DE. GLUT4 exocytosis. J Cell Sci 2011;124:4147–4159
3. Koonen DP, Glatz JF, Bonen A, Luiken JJ. Long-chain fatty acid uptake and FAT/CD36 translocation in heart and skeletal muscle. Biochim Biophys Acta 2005;1736:163–180
4. Coburn CT, Knapp FF Jr, Febbraio M, Beets AL, Silverstein RL, Abumrad NA. Defective uptake and utilization of long chain fatty acids in muscle and adipose tissues of CD36 knockout mice. J Biol Chem 2000;275:32523–32529
5. Holloway GP, Luiken JJ, Glatz JF, Spriet LL, Bonen A. Contribution of FAT/CD36 to the regulation of skeletal muscle fatty acid oxidation: an overview. Acta Physiol (Oxf) 2008;194:293–309
6. Liu L, Zhang Y, Chen N, Shi X, Tsang B, Yu YH. Upregulation of myocellular DGAT1 augments triglyceride synthesis in skeletal muscle and protects against fat-induced insulin resistance. J Clin Invest 2007;117:1679–1689
7. Pol A, Gross SP, Parton RG. Review: biogenesis of the multifunctional lipid droplet: lipids, proteins, and sites. J Cell Biol 2014;204:635–646
8. Romero MdelM, Roy S, Pouillot K, et al. Treatment of rats with a self-selected hyperlipidic diet, increases the lipid content of the main adipose tissue sites in a proportion similar to that of the lipids in the rest of organs and tissues. PLoS One 2014;9:e90995
9. Cao P, Fan SJ, Wang AM, et al. Diffusion magnetic resonance monitors intramyocellular lipid droplet size in vivo. Magn Reson Med 2015;73:59–69
10. Bosma M. Lipid droplet dynamics in skeletal muscle. Exp Cell Res 2016;340:180–186
11. Sato T, Mushiake S, Kato Y, et al. The Rab8 GTPase regulates apical protein localization in intestinal cells. Nature 2007;448:366–369
12. Sun Y, Bilan PJ, Liu Z, Klip A. Rab8A and Rab13 are activated by insulin and regulate GLUT4 translocation in muscle cells. Proc Natl Acad Sci U S A 2010;107:19909–19914
13. Randhawa VK, Ishikura S, Talior-Volodarsky I, et al. GLUT4 vesicle recruitment and fusion are differentially regulated by Rac, AS160, and Rab8A in muscle cells. J Biol Chem 2008;283:27208–27219
14. Samovski D, Su X, Xu Y, Abumrad NA, Stahl PD. Insulin and AMPK regulate FA translocase/CD36 plasma membrane recruitment in cardiomyocytes via Rab GAP AS160 and Rab8a Rab GTPase. J Lipid Res 2012;53:709–717
15. Farese RV Jr, Walther TC. Lipid droplets finally get a little R-E-S-P-E-C-T. Cell 2009;139:855–860
16. Guo Y, Walther TC, Rao M, et al. Functional genomic screen reveals genes involved in lipid-droplet formation and utilization. Nature 2008;453:657–661
17. Wu L, Xu D, Zhou L, et al. Rab8a-AS160-MSS4 regulatory circuit controls lipid droplet fusion and growth. Dev Cell 2014;30:378–393
18. Haldar M, Hancock JD, Coffin CM, Lessnick SL, Capecchi MR. A conditional mouse model of synovial sarcoma: insights into a myogenic origin. Cancer Cell 2007;11:375–388
19. Chen L, Chen Q, Xie B, et al. Disruption of the AMPK-TBC1D1 nexus increases lipogenic gene expression and causes obesity in mice via promoting IGF1 secretion. Proc Natl Acad Sci U S A 2016;113:7219–7224
20. Chen Q, Quan C, Xie B, et al. GARNL1, a major RalGAP α subunit in skeletal muscle, regulates insulin-stimulated RalA activation and GLUT4 trafficking via interaction with 14-3-3 proteins. Cell Signal 2014;26:1636–1648

21. Chen S, Wasserman DH, MacKintosh C, Sakamoto K. Mice with AS160/TBC1D4-Thr649Ala knockin mutation are glucose intolerant with reduced insulin sensitivity and altered GLUT4 trafficking. Cell Metab 2011;13:68–79
22. Dzamko N, Schertzer JD, Ryall JG, et al. AMPK-independent pathways regulate skeletal muscle fatty acid oxidation. J Physiol 2008;586:5819–5831
23. Chen Q, Xie B, Zhu S, et al. A Tbc1d1 Ser231Ala-knockin mutation partially impairs AICAR- but not exercise-induced muscle glucose uptake in mice. Diabetologia 2017;60:336–345
24. Schoonjans K, Peinado-Onsurbe J, Lefebvre AM, et al. PPARalpha and PPARgamma activators direct a distinct tissue-specific transcriptional response via a PPRE in the lipoprotein lipase gene. EMBO J 1996;15:5336–5348
25. Michaud SE, Renier G. Direct regulatory effect of fatty acids on macrophage lipoprotein lipase: potential role of PPARs. Diabetes 2001;50:660–666
26. Glatz JF, Luiken JJ. From fat to FAT (CD36/SR-B2): understanding the regulation of cellular fatty acid uptake. Biochimie 2017;136:21–26
27. Brown MS, Goldstein JL. The SREBP pathway: regulation of cholesterol metabolism by proteolysis of a membrane-bound transcription factor. Cell 1997;89:331–340
28. Shimano H, Yahagi N, Amemiya-Kudo M, et al. Sterol regulatory element-binding protein-1 as a key transcription factor for nutritional induction of lipogenic enzyme genes. J Biol Chem 1999;274:35832–35839
29. Porstmann T, Santos CR, Griffiths B, et al. SREBP activity is regulated by mTORC1 and contributes to Akt-dependent cell growth. Cell Metab 2008;8:224–236
30. Owen JL, Zhang Y, Bae SH, et al. Insulin stimulation of SREBP-1c processing in transgenic rat hepatocytes requires p70 S6-kinase. Proc Natl Acad Sci U S A 2012;109:16184–16189
31. Peterson TR, Sengupta SS, Harris TE, et al. mTOR complex 1 regulates lipin 1 localization to control the SREBP pathway. Cell 2011;146:408–420
32. Fang Y, Vilella-Bach M, Bachmann R, Flanigan A, Chen J. Phosphatidic acid-mediated mitogenic activation of mTOR signaling. Science 2001;294:1942–1945
33. Arous C, Naïmi M, Van Obberghen E. Oleate-mediated activation of phospholipase D and mammalian target of rapamycin (mTOR) regulates proliferation and rapamycin sensitivity of hepatocarcinoma cells. Diabetologia 2011;54:954–964
34. Su X, Abumrad NA. Cellular fatty acid uptake: a pathway under construction. Trends Endocrinol Metab 2009;20:72–77
35. Rector RS, Thyfault JP. Does physical inactivity cause nonalcoholic fatty liver disease? J Appl Physiol (1985) 2011;111:1828–1835
36. Keating SE, Hackett DA, George J, Johnson NA. Exercise and non-alcoholic fatty liver disease: a systematic review and meta-analysis. J Hepatol 2012;57:157–166
37. Bacchi E, Negri C, Targher G, et al. Both resistance training and aerobic training reduce hepatic fat content in type 2 diabetic subjects with nonalcoholic fatty liver disease (the RAED2 Randomized Trial). Hepatology 2013;58:1287–1295
38. Goodpaster BH, He J, Watkins S, Kelley DE. Skeletal muscle lipid content and insulin resistance: evidence for a paradox in endurance-trained athletes. J Clin Endocrinol Metab 2001;86:5755–5761